Model-measurement comparison of mesospheric temperature inversions, and a simple theory for their occurrence

Article

Published Version

It is advisable to refer to the publisher's version if you intend to cite from the work. See Guidance on citing.

www.reading.ac.uk/centaur

CentAUR

Central Archive at the University of Reading

Reading's research outputs online

Model-measurement comparison of mesospheric temperature inversions, and a simple theory for their occurrence

R. J. Sica,[1] P. S. Argall,[1] T. G. Shepherd,[2] and J. N. Koshyk[2,3]

[1] Mesospheric temperature inversions are well established observed phenomena, yet their properties remain the subject of ongoing research. Comparisons between Rayleigh-scatter lidar temperature measurements obtained by the University of Western Ontario's Purple Crow Lidar (42.9°N, 81.4°W) and the Canadian Middle Atmosphere Model are used to quantify the statistics of inversions. In both model and measurements, inversions occur most frequently in the winter and exhibit an average amplitude of ∼10 K. The model exhibits virtually no inversions in the summer, while the measurements show a strongly reduced frequency of occurrence with an amplitude about half that in the winter. A simple theory of mesospheric inversions based on wave saturation is developed, with no adjustable parameters. It predicts that the environmental lapse rate must be less than half the adiabatic lapse rate for an inversion to form, and it predicts the ratio of the inversion amplitude and thickness as a function of environmental lapse rate. Comparison of this prediction to the actual amplitude/thickness ratio using the lidar measurements shows good agreement between theory and measurements. **Citation:** Sica, R. J., P. S. Argall, T. G. Shepherd, and J. N. Koshyk (2007), Model-measurement comparison of mesospheric temperature inversions, and a simple theory for their occurrence, *Geophys. Res. Lett.*, *34*, L23806, doi:10.1029/2007GL030627.

1. Introduction

[2] Temperature inversions on the order of a few to tens of degrees occur routinely in the mesosphere and lower thermosphere [e.g., *Schmidlin*, 1976; *Hauchecorne et al.*, 1987]. The inversions vary with season and latitude, and can have considerable temporal variability related to the phase of the tides [*Sica et al.*, 2002]. *Meriwether and Gerrard* [2004] provide a recent review of the relevant observations as well as of the various mechanisms that have been proposed for the formation of inversions in this region, noting the differences between inversions observed above and below the mesopause. Despite the considerable progress made in recent years, *Meriwether and Gerrard* [2004] state that "the formation mechanisms [of mesospheric inversions] remain poorly understood", and "no one theory

consistently and satisfactorily describes all the features observed."

[3] In this study, simulations from the Canadian Middle Atmosphere Model (CMAM) are examined for the occurrence of mesospheric inversions as a function of season at the model location nearest The University of Western Ontario's Purple Crow Lidar (42.9°N, 81.4°W). Eight years of lidar measurements are used to compile inversion statistics for comparison with three CMAM simulations, which are run under identical conditions except for their parameterization of gravity wave drag. This comparison allows us to assess the realism of mesospheric inversions in CMAM, and draw conclusions about their formation mechanism. A simple theory of mesospheric inversions with no adjustable parameters is developed, which is tested against the lidar measurements.

2. CMAM Simulations

[4] The Canadian Middle Atmosphere Model is a comprehensive three-dimensional general circulation model extending from Earth's surface to about 95 km altitude [*Beagley et al.*, 1997]. For the runs analyzed here, the vertical resolution in the mesosphere is about 2.25 km, with a horizontal grid spacing of about 375 km. The model is run without interactive chemistry. Sea surface temperatures are specified from a monthly mean climatology. The model includes a full representation of tropospheric physics including a boundary layer scheme and both deep and shallow convective parameterizations. The model thus simulates an active spectrum of resolved gravity waves [*Koshyk et al.*, 1999; *Manson et al.*, 2002; *Horinouchi et al.*, 2003] in addition to parameterizing the effects of unresolved gravity waves. For the latter, orographically forced waves are parameterized using the scheme of *McFarlane* [1987], but such waves should have a small effect on the local dynamics near Southern Ontario. In the three runs considered here the effects of non-orographic gravity waves are parameterized by one of two schemes, either the nonlinear spectral diffusion scheme of *Medvedev and Klaassen* [1995] or the Doppler spread scheme of *Hines* [1997], or are not parameterized at all. In the first two cases, the resulting zonal mean zonal wind fields are given by *Medvedev et al.* [1998] and *McLandress* [1998], respectively, and exhibit a zonal wind reversal around the mesopause; in the latter case they are given by *Beagley et al.* [1997], and exhibit no zonal wind reversal. The model fields were saved every three hours for one year from each simulation; this save interval is sufficient to resolve the temporal variability because the time integration scheme severely damps motions of higher frequencies [*Manson et al.*, 2002]. For consistency with the lidar measurements, the model temperature profiles used

[1]Department of Physics and Astronomy, The University of Western Ontario, London, Ontario, Canada.
[2]Department of Physics, University of Toronto, Toronto, Ontario, Canada.
[3]Now at TD Securities, Toronto, Ontario, Canada.

Table 1. Distribution of Suitable Purple Crow Lidar Measurements by Month, 1997–2004

Month	Number of Nights	Number of Inversions, $\Delta z = 2$ km	Number of Inversions, $\Delta z = 480$ m
January	5	4	5
February	12	10	8
March	13	10	13
April	19	6	16
May	51	2	27
June	51	9	27
July	51	19	40
August	71	31	57
September	29	10	28
October	32	16	24
November	19	15	15
December	13	11	10

Figure 1. Histograms of the inversion frequency for the three CMAM simulations and the PCL measurements binned by month at 2 km vertical resolution. "cl" is the run with only the orographic gravity-wave parameterization; "Mk" also uses the Medvedev-Klaassen non-orographic parameterization, while "Hi" uses the Hines non-orographic parameterization.

were the average temperature profile between 0300 and 0900 UT, consistent with the typical range in universal time of the lidar measurements.
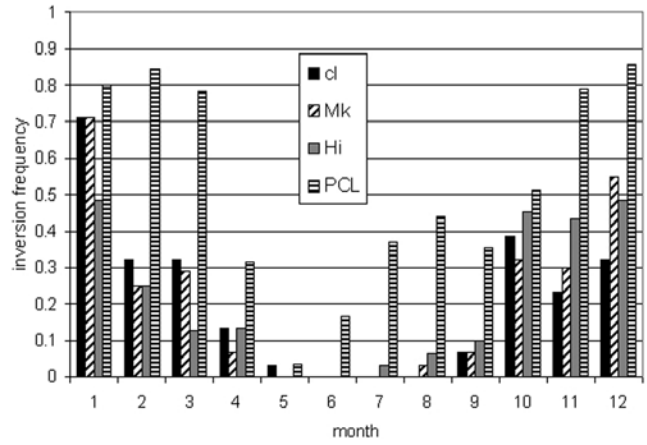
3. Purple Crow Lidar

[5] To study the properties of mesospheric inversion layers requires high vertical resolution temperature measurements. Such measurements were obtained using the Purple Crow Lidar Rayleigh-scatter system [*Sica et al.*, 1995]. The temperature analysis employed is based on the scheme described by *Chanin and Hauchecorne* [1984] with a correction for ozone as given by *Sica et al.* [2001]. The temperature analysis requires the choice of a seed temperature at the top of the profile, whose contribution to the total error is not known precisely without an independent knowledge of the true temperature. However, the seeding has only a small effect on the nightly-averaged mesospheric temperatures, as the temperature retrievals begin well above the mesopause.

[6] For consistency with the model the nightly averaged temperature profiles were processed with a vertical resolution of 1 km, with no additional smoothing, and then coadded to 2 km. The distribution of PCL measurements by month for the 366 nights used in this study is shown in Table 1. Useful measurements (e.g. signal-to-noise ratio greater than 4.5) were obtained up to at least 95 km on all nights used in this study.

[7] The amplitude, height and thickness of the inversions were found in a manner similar to that of *Leblanc and Hauchecorne* [1997]. To be counted as an inversion the increase in temperature with height must be greater than 1 K. This criterion results from the largest nominal statistical error of the lidar temperature measurements near the mesopause, about 0.5 K. The amplitude is then the total increase in temperature, the height of the inversion is the mean altitude and the thickness the altitude change from the beginning to the end of the inversion. Each night of lidar measurements was checked to insure that the inversion height determined by the above procedure was below the height of the mesopause on that night.

4. CMAM Results

[8] Figure 1 shows the frequency of inversions for each of the three model simulations (as well as the Purple Crow Lidar measurements, discussed below). The inversion fre-

quency is defined as the fraction of the total number of temperature profiles in the month exhibiting one or more inversions. The frequency of inversions in CMAM is maximum in the winter (25 to 70% of the nights) and nearly zero in the summer.

[9] Figure 2 shows that the amplitude of the inversions in CMAM ranges from 5 to 10 K in the winter and is below 5 K in spring and autumn. The altitude of the inversions occurs between 65 and 70 km, with the lowest altitudes in winter, and with a tendency for the inversions to be thicker in winter.

[10] All three simulations yield similar inversion statistics. Hence, the CMAM inversions appear to be associated
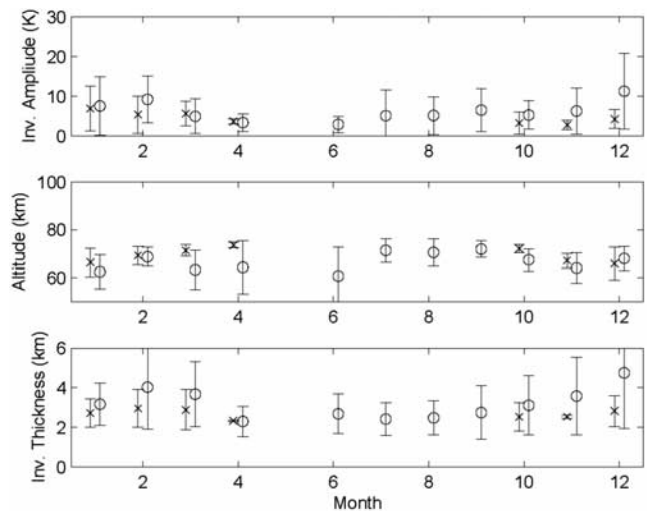
Figure 2. Direct comparison of the inversion amplitude, altitude, and thickness between the CMAM calculations (x's) and the PCL measurements (circles) at 2 km vertical resolution. The vertical bars show the standard deviation about the average value for the month.

with the resolved structures in the model, and not with the effects of parameterized gravity waves. This is an important result in itself. Furthermore, *Sassi et al.* [2002] argued that the mesospheric inversions found in the WACCM general circulation model were the result of planetary wave breaking in a mesospheric "surf zone" associated with a zero zonal-wind line. While this might be true for WACCM, the CMAM results show that such a scenario is not a necessary condition for mesospheric inversions, since the run with only orographic gravity-wave drag does not have a zonal wind reversal. In any case, such a mechanism cannot explain inversion layers in the half of the year when stratospheric winds are easterly. Hereafter, only results from the run with just orographic gravity-wave drag will be shown.

5. PCL Results

[11] The number of inversions in each month is listed in Table 1, while Figure 1 shows the inversion frequency. The inversion frequency is greater than 50% in November to March, with fewer inversions seen in April to June. Multiple inversions are mostly seen in October to April, with a few cases in the summer. While the overall seasonality in inversion frequency is similar to that seen in the CMAM, the lidar measurements show a considerable number of inversions between June and September, consistent with earlier observational studies [e.g., *Hauchecorne et al.*, 1987].

[12] Figure 2 shows the characteristics of the PCL inversions. The variability of the inversion parameters is large, but the inversions are clearly of larger amplitude in the winter than the summer. The altitude of the inversions is about 5 km higher in July to October compared to the rest of the year. The inversion height increases as the mesopause height decreases, and inversions tend to occur nearer to the mesopause in the July to October period.

6. A Simple Theory for the Inversions

[13] Lidar measurements at midlatitudes [*Whiteway et al.*, 1995; *Duck et al.*, 2001] have shown that the topsides of mesospheric inversion layers have a temperature structure that is close to adiabatic. This is what one would expect for a wave that is saturated according to the condition for convective instability, the presumption being that any superadiabatic lapse rate would immediately be removed by convective adjustment. This situation is certainly the case in general circulation models. Such a saturation hypothesis is the basis of *Lindzen*'s [1981] parameterization of gravity-wave breaking, but it is reasonable to assume that any atmospheric wave (e.g. a tide or a planetary wave) likewise cannot support a superadiabatic lapse rate. We now explore the implications of this line of reasoning.

[14] Consider an upward propagating wave, which will grow in amplitude as it propagates into regions of decreasing air density. We consider the mesosphere, where the background temperature decreases with altitude. Assume the wave has sufficient amplitude to saturate in the mesosphere and that the wave's saturation is determined by the condition for static stability. Then the sum of the environ-
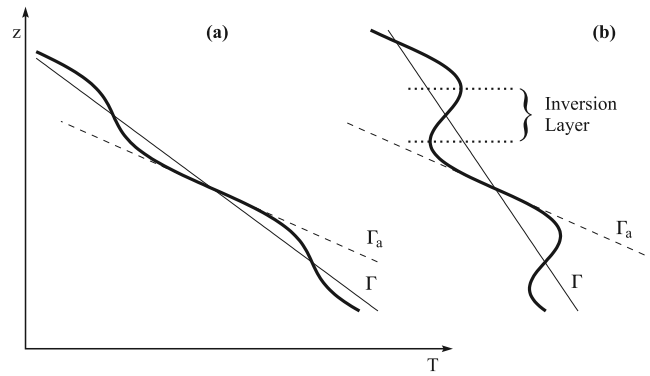

Figure 3. Schematic showing the temperature profile (thick black line) associated with a saturated wave. Γ denotes the profile associated with the environmental lapse rate, and Γ_a that associated with the dry adiabatic lapse rate. (a) The environmental lapse rate is sufficiently large that a saturated wave does not lead to an inversion. (b) The environmental lapse rate is less than $\Gamma_a/2$ (see condition (3)) and an inversion occurs.

mental lapse rate, Γ, and the perturbation of Γ due to the wave, $-\partial T'/\partial z$, cannot exceed the dry adiabatic lapse rate Γ_a, so that at saturation

$$\Gamma_a = \Gamma + (-\partial T'/\partial z)_{max}. \tag{1}$$

[15] The minimum lapse rate at saturation is then achieved 180 degrees out of phase, namely

$$\Gamma - (-\partial T'/\partial z)_{max} = 2\Gamma - \Gamma_a. \tag{2}$$

[16] For an inversion to form, the minimum lapse rate must be less than zero. The condition for an inversion to form is then

$$\Gamma < \frac{\Gamma_a}{2}. \tag{3}$$

[17] If the background lapse rate Γ is too large, then a saturated wave does not lead to an inversion (Figure 3a). However, if the background lapse rate satisfies (3), then a saturated wave results in an inversion layer (Figure 3b). Note that this condition contains no adjustable parameters.

[18] Now assume a saturated wave with a vertical wavenumber k. It follows from (1) that the peak-to-peak temperature amplitude of the wave is $2(\Gamma_a - \Gamma)/k$. When (3) is satisfied the following expressions can be obtained for the inversion amplitude ΔT and the inversion thickness Δz:

$$\Delta T = 2[(\Gamma_a - \Gamma)/k] \sin\{\cos^{-1}[\Gamma/(\Gamma_a - \Gamma)]\} \\ - 2(\Gamma/k) \cos^{-1}[\Gamma/(\Gamma_d - \Gamma)], \tag{4}$$

$$\Delta z = (2/k) \cos^{-1}[\Gamma/(\Gamma_a - \Gamma)]. \tag{5}$$

[19] Although k may be poorly defined by the measurements, it turns out that the ratio of ΔT to Δz is independent of k. The ratio is then

$$\frac{\Delta T}{\Delta z} = \frac{(\Gamma_a - \Gamma)\sin\{\cos^{-1}[\Gamma/(\Gamma_a - \Gamma)]\} - \Gamma\cos^{-1}[\Gamma/(\Gamma_a - \Gamma)]}{\cos^{-1}[\Gamma/(\Gamma_a - \Gamma)]}. \tag{6}$$

[20] As with (3), this prediction contains no adjustable parameters. If we approximate the right-hand side of (6) by a Taylor expansion, assuming $\Gamma/(\Gamma_a - \Gamma) \approx 1$, then the ratio of the inversion amplitude to thickness (henceforth, the inversion ratio) simplifies to:

$$\frac{\Delta T}{\Delta z} = \frac{2}{3}(\Gamma_a - 2\Gamma). \tag{7}$$

[21] Since the PCL measures the inversion amplitude, thickness and temperature profile at sufficiently high vertical resolution, the lidar's measurements of Γ can be used to predict the ratio $\Delta T/\Delta z$ from either (6) or (7), and the result compared with the observed $\Delta T/\Delta z$. Unfortunately, the CMAM calculations cannot be treated in a similar manner, as the model vertical resolution at these altitudes (about 2.25 km) is too coarse to be able to perform a meaningful estimate of the inversion ratio, as described in the next section.

7. Comparison of the CMAM Calculations and PCL Measurements to the Theoretical Predictions

[22] The first comparison that can be made between the measurements, model and simple theory is the inversion condition (3). Figure 4a shows the lapse rate from 60 to 80 km determined directly from monthly-averaged temperature profiles (which do not show inversion features) for both the CMAM and the PCL measurements, together with one-half the adiabatic lapse rate, which is shown as the dashed horizontal line. The mean measured and modeled lapse rates are in extremely good agreement with each other. Evidently mesospheric inversions are always possible according to condition (3). However, the mean lapse rates are much smaller in the winter than in the summer, which according to the theory is consistent with stronger and more frequent inversions in the winter.

[23] To compare the PCL measurements to the predicted ratio of the inversion amplitude to thickness, we no longer smooth the PCL measurements to the CMAM resolution; note the theoretical prediction does not depend on vertical resolution. It was determined that a vertical resolution of 480 m offered the best trade-off between resolution and signal-to-noise ratio of the retrieved temperature. This higher resolution resolves more inversions overall compared to Figure 1 (Table 1). A linear regression is then computed to determine the inversion ratio, using the inversion amplitudes as a function of thickness (Figure 4b). The errors in this determination are those of the regression line's slope. The measured ratio can then be compared to the ratio calculated from the exact expression (6) and the approximation (7), both determined using the monthly average Γ measured by the PCL.
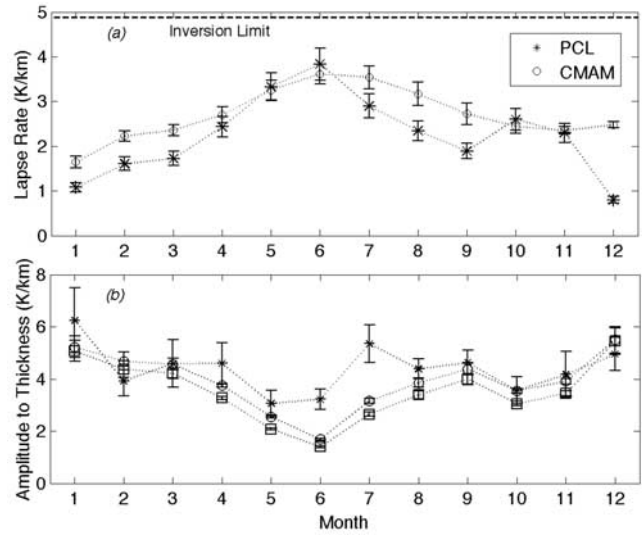

Figure 4. (a) Mean environmental lapse rate between 60 and 80 km altitude as a function of month from the PCL measurements and the CMAM simulations. The dashed "Inversion Limit" line is at half the adiabatic lapse rate, the maximum value for which an inversion can form. The vertical lines show the RMS variation about the monthly mean lapse rate. (b) Monthly-averaged inversion amplitude to thickness determined from the PCL measurements (asterisks) at 480 m vertical resolution. The vertical bars show the error in the slope of the ΔT versus Δz regression line. Predicted amplitude to thickness ratios calculated from the exact expression (6) (circles) and the approximation (7) (squares) using the monthly-averaged PCL lapse rate measurements are also shown, with the vertical bar indicating the RMS variation due to variability in the monthly mean lapse rate.

[24] For most months, the agreement between the regression fits and (6) is excellent, the exceptions being June and July where the inversion ratio predicted by the lidar-derived lapse rate appears to be too small compared to the observed ratio. The approximation (7) underestimates the exact expression (6) by about 10%.

8. Conclusions

[25] Eight years of PCL Rayleigh-scatter temperature measurements have been used to characterize the features of mesospheric inversions. These statistics have been compared to CMAM model calculations of the temperature climatology at the closest model grid point using three different types of parameterization for non-orographic gravity waves.

[26] The mesospheric inversions simulated in the CMAM have characteristics similar to the inversions measured by the PCL. The inversions in the CMAM result from the model's resolved features, as changing the parameterization of non-orographic gravity waves in the model does not significantly change the nature of the inversions. Nor are the inversion statistics particularly sensitive to the presence or absence of a zonal-wind reversal in the mesosphere. Thus, the mechanism identified by *Sassi et al.* [2002] for meso-

spheric inversions in the WACCM is not a necessary condition for mesospheric inversions.

[27] A simple theory of the inversions due to wave saturation is developed, with no adjustable parameters, and is shown to be consistent with the PCL measurements. The mesospheric inversions thus appear to be a signature of wave saturation in the mesosphere, which is consistent with the observation by *Whiteway et al.* [1995] that mesospheric inversions are capped by an adiabatic layer. While *Whiteway et al.* [1995] argued that the mixing associated with saturation was the cause of the inversion layer, our interpretation is rather that inversion layers result from the waves themselves, but their properties are constrained by saturation. The saturating waves can be gravity waves (for CMAM, resolved gravity waves), tides, planetary waves or a combination of these wave types.

[28] According to the simple theory, CMAM's environmental lapse rate is capable of supporting mesospheric inversions in the summer. The near absence of summertime inversions in CMAM therefore points to an absence of the relevant saturating waves. The likely culprits would seem to be either small-scale gravity waves unresolved by the CMAM, or the non-migrating diurnal tide.

References

Beagley, S. R., J. de Grandpré, J. N. Koshyk, N. A. McFarlane, and T. G. Shepherd (1997), Radiative-dynamical climatology of the first-generation Canadian Middle Atmosphere Model, *Atmos. Ocean*, *35*, 293–331.

Chanin, M. L., and A. Hauchecorne (1984), Lidar studies of temperature and density using Rayleigh scattering, in *Handbook for MAP*, vol. 13, *Ground-Based Techniques*, paper 7, pp. 87–98, Sci. Comm. on Sol. Terr. Phys., Int. Counc. of Sci. Unions, Urbana, Ill.

Duck, T. J., D. P. Sipler, J. E. Salah, and J. W. Meriwether (2001), Rayleigh lidar observations of a mesospheric inversion layer during night and day, *Geophys. Res. Lett.*, *28*, 3597–3600.

Hauchecorne, A., M. L. Chanin, and R. Wilson (1987), Mesospheric temperature inversion and gravity wave breaking, *Geophys. Res. Lett.*, *14*, 933–936.

Hines, C. O. (1997), Doppler-spread parameterization of gravity-wave momentum deposition in the middle atmosphere: 1. Basic formulation, *J. Atmos. Sol. Terr. Phys.*, *59*, 371–386.

Horinouchi, T., S. Pawson, K. Shibata, U. Langematz, E. Manzini, F. Sassi, R. J. Wilson, K. P. Hamilton, J. de Grandpré, and A. A. Scaife (2003),

Tropical cumulus convection and upward propagating waves in middle atmospheric GCMs, *J. Atmos. Sci.*, *60*, 2765–2782.

Koshyk, J. N., B. A. Boville, K. Hamilton, E. Manzini, and K. Shibata (1999), The kinetic energy spectrum of horizontal motions in middle atmosphere models, *J. Geophys. Res.*, *104*, 27,177–27,190.

Leblanc, T., and A. Hauchecorne (1997), Recent observations of mesospheric temperature inversions, *J. Geophys. Res.*, *102*, 19,471–19,482.

Lindzen, R. S. (1981), Turbulence and stress owing to gravity wave and tidal breakdown, *J. Geophys. Res.*, *86*, 9707–9714.

Manson, A. H., et al. (2002), Gravity-wave activity and dynamical effects in the middle atmosphere (60–90 km): Observations from an MF/MLT radar network and results from the Canadian Middle Atmosphere Model (CMAM), *J. Atmos. Sol. Terr. Phys.*, *64*, 65–90.

McFarlane, N. A. (1987), The effect of orographically excited gravity wave drag on the general circulation of the lower stratosphere and troposphere, *J. Atmos. Sci.*, *44*, 1175–1800.

McLandress, C. (1998), On the importance of gravity waves in the middle atmosphere and their parameterization in general circulation models, *J. Atmos. Sol. Terr. Phys.*, *60*, 1357–1383.

Medvedev, A. S., and G. P. Klaassen (1995), Vertical evolution of gravity wave spectra and the parameterization of associated wave drag, *J. Geophys. Res.*, *100*, 25,841–25,853.

Medvedev, A. S., G. P. Klaassen, and S. R. Beagley (1998), On the role of an anisotropic gravity-wave spectrum in maintaining the circulation of the middle atmosphere, *Geophys. Res. Lett.*, *25*, 509–512.

Meriwether, J. W., and A. J. Gerrard (2004), Mesospheric inversion layers and stratosphere temperature enhancements, *Rev. Geophys.*, *42*, RG3003, doi:10.1029/2003RG000133.

Sassi, F., R. R. Garcia, B. A. Boville, and H. Liu (2002), On temperature inversions and the mesospheric surf zone, *J. Geophys. Res.*, *107*(D19), 4380, doi:10.1029/2001JD001525.

Schmidlin, F. J. (1976), Temperature inversions near 75 km, *Geophys. Res. Lett.*, *3*, 173–176.

Sica, R. J., S. Sargoytchev, P. S. Argall, E. F. Borra, L. Girard, C. T. Sparrow, and S. Flatt (1995), Lidar measurements taken with a large-aperture liquid mirror: 1. Rayleigh-scatter system, *Appl. Opt.*, *34*, 6925–6936.

Sica, R. J., Z. A. Zylawy, and P. S. Argall (2001), Ozone correction for Rayleigh-scatter temperature determinations in the middle atmosphere, *J. Atmos. Oceanic Technol.*, *18*, 1223–1228.

Sica, R. J., T. Thayaparan, P. S. Argall, A. T. Russell, and W. K. Hocking (2002), Modulation of upper mesospheric temperature inversions due to tidal-gravity wave interactions, *J. Atmos. Sol. Terr. Phys.*, *64*, 915–922.

Whiteway, J. A., A. I. Carswell, and W. E. Ward (1995), Mesospheric temperature inversions with overlying nearly adiabatic lapse rate: An indication of a well-mixed turbulent layer, *Geophys. Res. Lett.*, *22*, 1201–1204.

————————————

P. S. Argall and R. J. Sica, Department of Physics and Astronomy, The University of Western Ontario, London, ON, Canada N6A 3K7. (sica@physics.uwo.ca)

J. N. Koshyk, TD Securities, 222 Bay Street, 7th Floor, Toronto, ON, Canada M5K 1A2.

T. G. Shepherd, Department of Physics, University of Toronto, 60 St. George Street, Toronto, ON, Canada M5S 1A7.